Stress measurement in the iron oxide scale formed on pure Fe during isothermal transformation by in situ high-temperature X-ray diffraction

Shigenari Hayashi[1], Yurika Yamanouchi[2], Kosuke Hayashi[3], Yasuyoshi Hidaka[3], and Masugu Sato[4]

1: Division of Materials Science and Engineering, Faculty of Engineering, Hokkaido University, N13, W8, Kitaku, Sapporo, Hokkaido, 060-8628, Japan
2: Technical Service Division, Technical Center, Faculty of Engineering, Hokkaido University, N13, W8, Kitaku, Sapporo, Hokkaido, 060-8628, Japan
3: Process Research Laboratories, Nippon Steel Corporation, Amagasaki, Hyogo, 660-0891, Japan
4: Japan Synchrotron Radiation Research Institute, Sayo-gun, Hyogo, 679-5198, Japan

Abstract

The stress development in the iron oxide scale formed on pure Fe during isothermal oxidation at 700 °C followed by isothermal transformation at 500 or 380 °C was measured by in situ high-temperature X-ray diffraction with the $\sin^2\psi$ method. The eutectoid transformation resulted in compressive stress generation in the Fe_3O_4 and Fe in the eutectoid structure. This compressive stress was relaxed during the isothermal heat treatment after the eutectoid reaction. The stress generation was ascribed primarily to volume changes associated with the oxidation and/or reduction of the iron oxide at the interfaces, Fe_3O_4 precipitation, and the eutectoid reaction.

Keywords: Iron oxide scale, $\sin^2\psi$ method, in situ high-temperature stress measurement

Introduction

The phase transformation of the iron oxide scale that forms on hot-rolled steel strips during cooling is one of the most important phenomena determining the surface quality of the strips because the properties of the oxide scale, such as spallation resistance, crack initiation and propagation, and pickling behaviour, are strongly dependent on the scale microstructure. To obtain steel strips with high surface quality it is crucial to understand the microstructural development of the iron oxide scale, which consists of thin layers of Fe_2O_3 and Fe_3O_4 and a thick layer of FeO, during phase transformation. Numerous studies have been conducted to examine the isothermal phase transformation behaviour of the iron oxide scales formed on pure Fe, Fe–Mn alloys, and low-carbon steels, and mechanisms for the phase transformation of thermally grown oxide scales have been proposed and discussed [1–14].

The properties of the oxide scale are also influenced by the residual stress that develops in the scale during oxidation and phase transformation. It is well known that this residual stress is generated through several mechanisms, including the growth of the oxide scale (growth stress), heating and cooling after oxidation (thermal stress), and phase transformation (transformation stress). Several studies have been performed to measure the residual stress that develops during

the oxidation of pure Fe or steels under various atmospheres and the isothermal transformation of oxide scales [15–20]. In these studies, the stress development was evaluated using the "flexure method" or X-ray diffraction (XRD) with the $\sin^2\psi$ technique.

In the flexure method, the bending behaviour of a thin ribbon-shaped specimen coated on one surface with Ni or SiO_2 is monitored during oxidation to evaluate the stress generation. For example, Tanei and Kondo examined the compressive stress development in the oxide scale during the phase transformation of FeO at 400 °C [17]. Taniguchi et al. recognized the compressive stress generation in the FeO layer near Fe_3O_4/FeO and FeO/Fe substrate interfaces during oxidation in O_2 [16]. However, the flexure method only provides the overall stress development in the oxide scale and does not permit evaluation of the stress development in the different oxide layers and phases. In contrast, XRD analysis with the $\sin^2\psi$ technique reveals the stress generation in specific phases.

The stress measurement by XRD with the $\sin^2\psi$ technique is commonly used to evaluate the residual stress generated near the surface region of surface modified materials by coating, shot-peening, and carburization so on. However, relatively long measurement time is required for residual stress analysis by $\sin^2\psi$ technique since one analysis consists of several measurements of the diffraction signals at various ψ angles to obtain the change in d-spacing with different ψ angles to evaluate the residual stress. Thus, the $\sin^2\psi$ technique was not suitable for in situ stress measurement when a high time resolution is required for the analysis. However, in situ high-temperature XRD (HTXRD) combined with a 2D detector allows to analyse dynamic phenomena such as the phase transformation of Al_2O_3 scale with a high time resolution [21, 22]. Thus, the $\sin^2\psi$ measurement combined with a 2D detector can allow an in situ measurement of the stress generation in the oxide scale during oxidation followed by phase transformation with a relatively high time resolution.

Sasaki et al. measured the residual stress generation in the oxide scale formed on steel containing 0.1 wt % C and 1 wt % Si at 900 °C during cooling to room temperature in Ar by means of synchrotron source combined with 2D detector [20]. According to their analysis, no stress development occurred in the FeO during cooling to 700 °C, then compressive thermal stress developed during cooling to 600 °C. Further cooling to 500 °C caused the compressive stress to transition to tensile stress, which was ascribed to the precipitation of Fe_3O_4 in the FeO. However, FeO is not a good oxide for measuring the stress generation in iron oxide scale because it is a non-stoichiometric oxide, $Fe_{1-x}O$, with a very large range of x. To measure the stress in the oxide scale by the $\sin^2\psi$ method, the measurement conditions must be judiciously selected such that the d-spacing of each oxide phase changes with the stress generation, i.e., the factors influencing the lattice constant, such as oxide composition and temperature, must be eliminated during the $\sin^2\psi$ measurements.

In this study, in situ HTXRD analysis of the Fe_3O_4 component was applied to elucidate the stress development in the iron oxide scale formed on high-purity Fe during oxidation followed by isothermal transformation.

Experimental Procedures

Samples with dimensions of 15 × 20 × 1[t] mm^3 were cut from a pure Fe sheet (>99.99%, Nilaco Corporation) and normalized at 920 °C for 20 min under vacuum to remove the strain and elongated grain structure introduced by cold rolling during production. The samples were then ground to a 1200-grit finish using SiC abrasive paper then ultrasonically cleaned in acetone prior to oxidation and the isothermal transformation tests. A diffractometer equipped with a rotary anticathode X-ray tube was used for the stress measurements.

<In situ stress measurement by the $\sin^2\psi$ method>

In situ HTXRD measurements were performed using an X-ray diffractometer (SmartLab, Rigaku) with Co Kα radiation (λ = 0.179278 nm). The X-ray beam (rotating anticathode tube, 40 keV, 135 mA) was focused by a converting optical tool (CBO-f, Rigaku) to a beam diameter of approximately 2 mm. The sample was placed on the heating stage of the infrared image furnace (Reactor X, Rigaku) attached to the goniometer. The diffraction signals were collected using a two-dimensional X-ray detector (HyPix-3000, Rigaku) positioned at a 2θ angle of 110° with a camera length of 149.5 mm. The sample was heated to 700 °C in static air at a rate of 50 °C/min followed by isothermal oxidation for 15 min to form an oxide scale with a thickness of approximately 30 μm. After formation of the oxide scale, the sample was cooled to 380 °C at a rate of 50 °C/min and subsequently held for up to 120 min for the isothermal transformation in static air. Some samples were maintained at 500 °C for 4 h prior to cooling to 380 °C. The oxidation and isothermal transformation conditions are schematically depicted in Fig. 1. The sample temperature was monitored using a Pt-13Rh thermocouple spot welded on the sample surface. The stress in the oxide scale was analysed by the $\sin^2\psi$ method using the Fe_3O_4(008) reflection. The diffraction signals from the oxide scale at various ψ angles (ψ = 0°, 5°, 10°, 15°, 17°, 20°, 22°, 24°, and 0°) were recorded for 10 s each in this order. The final measurement at ψ = 0° was performed to confirm that the lattice constant did not change during each series of stress measurements. The series of measurements at various ψ angles (about 3 min for the series including the movement time of the goniometer) was performed without the use of an interval until the end of the experiment. Conventional in situ HTXRD analysis of the oxide scale during isothermal oxidation, cooling, and isothermal transformation was also performed for separate samples to confirm the progress of the formation and phase transformation of the oxide scale. In this analysis, the reflections from the oxide scale were recorded every 10 s by the two-dimensional detector.

Following these measurements, cross sections of the oxide scale were examined by scanning electron microscopy (SEM).

Results

<Phase transformation behaviour of the oxide scale by in situ XRD measurements>

Figure 2 presents the XRD patterns of the oxide scale obtained during isothermal oxidation at 700 °C for 15 min followed by isothermal transformation at 380 °C. The intensity of each oxide phase as a function of time is also plotted in Fig. 3a, and Fig. 3b shows a similar plot for a sample

subjected to heat treatment at 500 °C for 4 h prior to the isothermal transformation at 380 °C. The temperature profiles shown in Fig. 3 are the actual temperatures measured at the sample surface.

During heating to 700 °C, the reflection from Fe_3O_4 was first detected, followed by the observation of wüstite (denoted $Fe_{1-\delta}O$). The intensity of the $Fe_{1-\delta}O$ reflection gradually increased over time during the heating and isothermal oxidation stages then rapidly increased during the post-oxidation cooling step, before suddenly starting to decrease rapidly toward the end of the cooling step and the start of the isothermal transformation stage. For the samples cooled immediately to 380 °C without heat treatment at 500 °C, wüstite with a larger *d*-spacing (denoted $Fe_{1-\varepsilon}O$, where $\delta > \varepsilon$) appeared toward the end of the cooling stage. The intensity of the $Fe_{1-\varepsilon}O$ reflection increased during the first 10 min of the isothermal transformation stage then decreased rapidly, and this component disappeared completely within approximately 30 min of the isothermal transformation. The Fe reflection from the substrate disappeared during the oxidation stage but reappeared after approximately 15 min of the isothermal transformation. The intensity of this reflection gradually increased during the first 25 min of the isothermal transformation stage then remained constant, corresponding to the period over which the $Fe_{1-\varepsilon}O$ reflection decreased in intensity then disappeared. The intensity of the Fe_3O_4 reflection gradually increased during the isothermal oxidation and cooling stages and the first 12 min of the isothermal transformation stage then increased at a faster rate, with the latter period corresponding to the time at which the Fe reflection was detected.

In the case of the samples maintained at 500 °C for 4 h prior to isothermal transformation at 380 °C, the $Fe_{1-\varepsilon}O$ reflection was not observed during the transformation at 500 °C (Fig. 3b). During this stage, the intensity of the $Fe_{1-\delta}O$ reflection gradually decreased while that for Fe_3O_4 gradually increased. However, upon cooling the samples to 380 °C, the intensity of the $Fe_{1-\delta}O$ peak rapidly decreased and the signal from $Fe_{1-\varepsilon}O$ appeared. The changes in the intensities of the Fe_3O_4, $Fe_{1-\varepsilon}O$, and Fe reflections with transformation time at 380 °C were very similar to those observed for the samples cooled immediately to 380 °C without heat treatment at 500 °C.

Figures 4 and 5 show cross-sectional SEM images of the oxide scales for the samples cooled immediately to 380 °C (Fig. 3a) and those subjected to intermediate heat treatment at 500 °C (Fig. 3b), respectively. In the former case, images were acquired at various time points during the oxidation and transformation stages, as indicated by the letters (i) to (iv) in Fig. 3a; in the latter case, the images were obtained after the transformation. At the end of the oxidation stage (point (i)), the oxide scale was composed of an outer Fe_3O_4 layer and an inner wüstite layer (Fig. 4a). A thin layer of Fe_2O_3 was presumably formed above the Fe_3O_4 layer, although this could not be observed in the conventional SEM image. During the cooling stage and at the start of the isothermal transformation stage (points (ii) and (iii)), some Fe_3O_4 precipitates were formed in the outer region of the wüstite layer (Figs. 4b and 4c). Some areas in the vicinity of the Fe_3O_4 precipitates had also undergone transformation to an Fe/Fe_3O_4 eutectoid structure, as indicated by the arrows in Fig. 4e. As the isothermal transformation progressed (point (iv)), the remaining wüstite then completely transformed to the fully eutectoid structure (Fig. 4d). For the sample maintained at 500 °C prior to the isothermal transformation at 380 °C, the oxide scale formed a thick outer Fe_3O_4 layer (Fig. 5). An inner scale with the eutectoid structure was also observed,

which indicates that the outer Fe_3O_4 layer grew thicker without the eutectoid reaction during the heat treatment at 500 °C.

The sequence and mechanism of the transformation of thermally grown wüstite scale have been well summarized in the literature [1, 2, 6, 7]. When an $Fe_{1-\delta}O$ scale is cooled below 570 °C, the transformation begins with the following reaction to form Fe_3O_4 and $Fe_{1-\varepsilon}O$:

$$(1-4\varepsilon)Fe_{1-\delta}O \rightarrow (\delta-\varepsilon)Fe_3O_4 + (1-4\delta)Fe_{1-\varepsilon}O \ (\delta>\varepsilon) \quad (1)$$

where $Fe_{1-\delta}O$ contains a higher concentration of cation vacancies and forms in regions with high oxygen potential, i.e., near the Fe_3O_4/wüstite interface. During the phase transformation, reaction (1) occurs through the inward growth of the outer Fe_3O_4 layer and/or the precipitation of Fe_3O_4 in the outer region of the wüstite ($Fe_{1-\delta}O$) layer. The precipitation or growth of Fe_3O_4 is dependent on the transformation temperature, i.e., the degree of supercooling. During prolonged transformation, the Fe content in $Fe_{1-\varepsilon}O$ becomes supersaturated and the following eutectoid reaction occurs with termination of the transformation:

$$4Fe_{1-\varepsilon}O \rightarrow Fe_3O_4 + (1-4\varepsilon)Fe \quad (2)$$

The phase transformation behaviour observed in the present study clearly followed this sequence and the temperature dependence reported in our previous study [6–9]. The changes in the intensities of the $Fe_{1-\delta}O$ and $Fe_{1-\varepsilon}O$ peaks and the precipitation of Fe_3O_4 at points (ii) and (iii) in Figs. 3, 4b, and 4c and the termination of the transformation by the eutectoid reaction at point (iv) in Figs. 3 and 4d are well explained by reactions (1) and (2), respectively.

In this study the Fe_3O_4 layer may grow thicker by oxidation in the isothermal transformation stage in static air. However, evaluating the thickness of the Fe_3O_4 layer by the oxidation in the isothermal transformation stage from the microstructural observation was too difficult, since the growth kinetics of the Fe_3O_4 by oxidation at 380 and 500 °C are very low [23] and those by the transformation by reaction (1) was faster. Thus, the effect of oxidation in the isothermal transformation stage on the thickness of Fe_3O_4 layer and stress generation in this layer was ignored in the following sections.

<Changes in the *d*-spacings of the Fe_3O_4 and Fe phases during isothermal transformation>

Figure 6 presents the variation of the *d*-spacings of the Fe_3O_4(008), $Fe_{1-\delta}O$, $Fe_{1-\varepsilon}O$(004), and Fe(112) phases observed during the experiment. The dashed lines in these plots indicate the *d*-spacings for powder samples of Fe_3O_4 and Fe at different temperatures measured by HTXRD. No reference *d*-spacing is shown for wüstite because the *d*-spacing of this component is dependent on not only temperature but also composition. The *d*-spacing of the Fe_3O_4 phase was slightly lower than the reference during isothermal oxidation at 688 or 696 °C. Upon cooling the samples to 388 °C (Fig. 6a), the *d*-spacing of the Fe_3O_4 phase decreased to a value similar to the reference, but it then increased again until the appearance of Fe after approximately 20 min of transformation. The *d*-spacing subsequently decreased again and gradually approached a constant value, which

was still higher than the reference, over the remainder of the transformation period. The *d*-spacing for Fe was also slightly higher than the reference. A similar tendency was observed when the oxide scale was heat treated at 523 °C and cooled to 414 °C, where the *d*-spacing became comparable to the reference value immediately after cooling then increased for further heat treatment at both temperatures at 523 and 414 °C. Thus, the changes in the *d*-spacing of the oxide phases were identical during transformation at 388 and 414 °C, irrespective of whether the oxide scale was subjected to intermediate heat treatment at 523 °C.

<In situ stress measurements of the oxide scale during isothermal transformation>

Figure 7 shows the diffraction peaks of the Fe_3O_4(008) reflection at various ψ angles during the $\sin^2\psi$ measurements after isothermal transformation at 380 °C for approximately 20 and 40 min. The peak shift upon varying the ψ angle was small, although the peak position clearly shifted toward a higher 2θ angle in both cases.

In the $\sin^2\psi$ method, the stress in the oxide scale (σ_φ) can be calculated using the following equation:

$$\sigma_\phi = \left(\frac{E}{1+\nu}\right)\frac{\partial\frac{\Delta d}{d_0}}{\partial\sin^2\psi} \qquad (\Delta d = d_\psi - d_0) \tag{3}$$

where d_0 is the *d*-spacing of the plane in the absence of stress and d_ψ is the *d*-spacing of the lattice plane, which has a normal vector with the angle ψ to the normal vector of the plane parallel to the surface. *E* and *v* are the Young's modulus and Poisson's ratio of the diffraction plane, respectively. As the Young's modulus and Poisson's ratio of the diffraction plane at different temperatures are unknown, the gradient of equation (3), $M = \frac{\partial\frac{\Delta d}{d_0}}{\partial\sin^2\psi}$, was used instead of σ_φ to evaluate the stress in the present study.

Figure 8 presents the variation of the *d*-spacing of the Fe_3O_4(008) reflection as a function of $\sin^2\psi$ after various isothermal transformation times at 380 °C. Note that the gradients of these plots correspond to *M*. Until about the fourth measurement, corresponding to 16 min of isothermal transformation, the *d*-spacings recorded for the first and last (closed red circles) measurements with $\psi = 0$ were not in agreement. The *d*-spacing was always higher for the last measurement than for the first measurement. This disagreement of the *d*-spacing between the two measurements at $\psi = 0$ is considered to originate from the increase in the *d*-spacing of Fe_3O_4 during the transformation as discussed for Fig. 6. Thus, the positive gradient observed in Figs. 8a and 8b is not likely attributable solely to stress development in the oxide scale. Therefore, the results from first two measurement points (indicated by arrows in Fig. 9) are less accurate for the stress evaluation. Although the *d*-spacings for the last $\psi = 0$ measurements still tended to be higher until the fourth measurement, the negative gradient *M* can be adopted for the stress assessment.

Figure 9 shows the variation of the gradient *M* for the Fe_3O_4(008) and Fe(112) reflections over time during the oxidation and isothermal transformation stages. Although the data points are scattered, tensile stress was found to be introduced during the isothermal oxidation at 700 °C.

This tensile stress still remained after cooling to 380 °C, but it transitioned to compressive stress after approximately 10 min of phase transformation at 380 °C. The compressive stress increased with transformation time up to approximately 20 min, then stress relaxation occurred over the remainder of the experiment. Although an exact comparison between the changes in the microstructure, oxide phases, and stress development is difficult owing to the use of different specimens for each measurement and cross-sectional SEM image of the oxide scale, the increase in the compressive stress in Fe_3O_4 appears to correspond to the precipitation of Fe_3O_4 in the FeO layer and the eutectoid reaction. The relaxation of the compressive stress is likely due to the deformation of Fe in the eutectoid structure when the transformation reached completion, as compressive stress was also confirmed to develop in the Fe and increased in accordance with the increase in compressive stress in the Fe_3O_4 phase.

Figure 10 shows the change in the gradient *M* during heat treatment at 500 °C followed by isothermal transformation at 380 °C. During the heat treatment stage, tensile stress was introduced into the Fe_3O_4 layer. Upon cooling the sample to 380 °C, the stress development was similar to that observed for the sample cooled immediately to 380 °C without intermediate heat treatment, although the level of compressive stress was lower. The lower degree of compressive stress observed for the sample with intermediate heat treatment at 500 °C may be attributable to the residual tensile stress in the thick outer Fe_3O_4 layer, because the measured stress is the average value across the oxide scale.

Discussion

The development of stress in Fe_3O_4 scale and its changes over time during oxidation followed by isothermal phase transformation were successfully measured by in situ HTXRD. The results revealed that tensile stress developed during oxidation at 700 °C and subsequently transitioned to compressive stress during isothermal transformation. The results indicate that the eutectoid transformation was responsible for the compressive stress development. After the eutectoid reaction, relaxation of the compressive stress introduced into the oxide scale occurred upon longer heat treatment.

<Stress development during isothermal oxidation>

Stress development in an oxide scale during isothermal oxidation, i.e., “growth stress”, may be caused by the volume changes associated with the metal-to-oxide transition (Pilling–Bedworth model) or the formation of one oxide layer on another (multilayered oxide model), a vacancy concentration gradient across the oxide scale and condensation in the subsurface region of the metal substrate (vacancy model), lattice mismatch between the oxide and metal (epitaxial stress model), or changes in the oxide composition [24]. Mitchell et al. identified the occurrence of tensile stress in the Fe_3O_4 layer formed between an outer Fe_2O_3 layer and inner FeO layer and proposed that this stress was generated by a Pilling–Bedworth ratio of $V_{Fe(Fe2O3)}/V_{Fe(Fe3O4)} = 1.02$ at the Fe_2O_3/Fe_3O_4 interface and an anion volume ratio with unchanging oxygen positions of $V_{OFe3O4}/V_{OFe(1-\delta)O} = 0.94$ [18]. Same treatment was also reported by Juricic et al. [19]. Taniguchi et al. also observed tensile stress in the Fe_3O_4 layer below the outermost Fe_2O_3 layer during a thin-

strip bending experiment and explained the development of the tensile stress by the multilayered oxide model, in which the reactions shown in equations (4), (5), and (6) at the $Fe_3O_4/Fe_{1-\delta}O$ and Fe_2O_3/Fe_3O_4 interfaces were considered to generate 6.5%, 10.3%, and 2.0% of volume expansion, respectively [16]:

$$Fe_3O_4 \rightarrow 4Fe_{1-\delta}O + (1-4\delta)V_{Fe}^{2+} + (2-8\delta)h \quad (4)$$

$$12Fe_2O_3 \rightarrow 9Fe_3O_4 + V_{Fe}^{2+} + V_{Fe}^{3+} + 8h \quad (5)$$

$$2Fe_3O_4 \rightarrow 3Fe_2O_3 + V_O^{2-} + 2e \quad (6)$$

where V_{Fe}^{2+} and V_{Fe}^{3+} are cation vacancies and h and e denote a hole and an electron, respectively. Tensile stress generation in the Fe_3O_4 layer on a carbon steel was also confirmed by Corkovic and Pyzalla using in situ HTXRD measurements at 600 °C with $\sin^2\psi$ analysis [15]. These authors explained that the tensile stress development in the Fe_3O_4 layer was mainly attributable to volume changes at the Fe_2O_3/Fe_3O_4 and $Fe_3O_4/Fe_{1-\delta}O$ interfaces. All of these studies confirmed the introduction of tensile stress into the Fe_3O_4 layer during isothermal oxidation, which is in accordance with the results of the present study.

<Stress development during isothermal transformation>

The tensile stress that had been introduced into the Fe_3O_4 layer rapidly decreased after cooling to 380 °C and gradually transitioned to compressive stress after approximately 10 min of isothermal transformation. The compressive stress increased up to approximately 28 min and subsequently decreased with further heat treatment. The decrease in the tensile stress in the Fe_3O_4 occurred concomitantly with the start of Fe_3O_4 precipitation and the eutectoid reaction (Figs. 4a, 5c, and 5e), which suggests that the precipitation of Fe_3O_4 and the eutectoid reaction were responsible for the volume expansion in the $Fe_{1-\varepsilon}O$ layer.

The lattice constants and molar volumes of $Fe_{1-\delta}O$, $Fe_{1-\varepsilon}O$, and Fe_3O_4 at 380 °C calculated from the measured average *d*-spacings of the FeO(004) and Fe_3O_4(008) reflections in Fig. 8a were 0.432, 0.435, and 0.844 nm and 12.1, 12.4, and 45.2 cm^3/mol, respectively. Thus, the precipitation of Fe_3O_4 in $Fe_{1-\varepsilon}O$ according to equation (1) and the eutectoid reaction given by equation (2) caused approximately 0.5% and 3% volume expansion, respectively. The low-level compressive strain is expected to be generated in the Fe_3O_4 precipitates by precipitation in the wüstite near the $Fe_3O_4/Fe_{1-\varepsilon}O$ interface. As the strain measured by XRD is the average value across the entire oxide scale, the level of compressive strain in the Fe_3O_4 precipitates in the $Fe_{1-\varepsilon}O$ layer is insufficient to compensate for the tensile strain remaining in the outer Fe_3O_4 layer. However, the subsequent occurrence of the eutectoid reaction should result in the development of greater compressive strain due to the higher volume expansion of 3%, affording higher compressive stress in the Fe_3O_4 in the eutectoid region. The formation of a large amount of Fe_3O_4 in the eutectoid region may also contribute to the transition from tensile to compressive stress.

During the phase transformation at 500 °C, the outer Fe_3O_4 layer grew inwardly thicker. This inward growth of the outer Fe_3O_4 layer proceeded through equation (1), which is the opposite reaction to equation (4) in which the Fe_3O_4 layer was reduced in the vicinity of the $Fe_3O_4/Fe_{1-\delta}O$

interface owing to the growth of wüstite. This implies volume reduction in the Fe_3O_4 layer, leading to the generation of tensile stress in this layer as depicted in Fig. 10. The stress generated in the Fe_3O_4 decreased and transitioned to compressive stress with the occurrence of the eutectoid reaction. However, the compressive stress measured in these samples was much lower than that observed for the samples cooled immediately to 380 °C without intermediate heat treatment at 500 °C. This occurred owing to the thickness of the outer Fe_3O_4 layer containing the residual tensile stress, which greatly contributed to the average stress in the entire Fe_3O_4 phase in the oxide scale.

After the eutectoid reaction the relaxation of residual stress was observed during isothermal heat treatment. Similar relaxation behaviour of residual stress/strain in Fe by aging treatment at 400 °C was reported in the cold-drawing fully pearlitic steel [25]. Although the relaxation mechanism of strain in the pearlite structure was not addressed in this paper, creep or/and plastic deformation might be responsible for this relaxation [26]. The Young's modulus of the Fe(001) plane at 380 °C, E_{001}, was calculated to be approximately 122.9 GPa using the following equation [27] and the Young's modulus of polycrystalline Fe (E^* = 190 GPa) [28]:

$$E_{001} = 0.647 \times E^* \tag{7}$$

The maximum compressive stress introduced into the Fe during the isothermal transformation was calculated from the measured M values shown in Fig. 9 and the Poisson's ratio of the Fe(001) plane at room temperature ($\nu_{001} = 0.29$ [27]) to be approximately 262 MPa, which is slightly smaller than the stress in the oxide scale reported by Tanei and Kondo [17], albeit much larger than the yield stress of Fe of approximately 6–23 MPa at 380 °C [29, 30]. Thus, it is reasonable to consider that the stress relaxation in the oxide scale occurred by the plastic deformation of Fe in the eutectoid structure during the isothermal heat treatment.

Conclusions

The stress development in iron oxide scale during the isothermal oxidation and isothermal transformation of wüstite was successfully measured by in situ HTXRD using the $\sin^2\psi$ method. Tensile stress developed in the outer Fe_3O_4 layer during the isothermal oxidation and appeared to remain during isothermal transformation at 500 °C and 380 °C. However, compressive stress was generated by the precipitation of Fe_3O_4 and the eutectoid reaction in the wüstite layer. In particular, the eutectoid reaction was confirmed to generate greater compressive stress in the Fe_3O_4. The introduced compressive stress was relaxed by the plastic deformation of Fe in the eutectoid structure after the eutectoid reaction.

References

1. W.A. Fischer, A. Hoffmann, R. Shimada, Arch. Eisenhuttenwes, 27, (1956), 521.
2. N. Otsuka, T. Doi, Y. Hidaka, Y. Higashida, Y. Masaki, N. Mizui and M. Sato, ISIJ int. 53, (2013), 286.
3. Z-F. Li, G-M. Cao, F. Lin, C-Y. Cui, H. Wang, and Z-Y Liu, ISIJ int., 58, (2018), 2338.

4. Z-F. Li, G-M. Cao, F. Lin, H. Wang, and Z-Y Liu, Oxid. Met., 90, (2018), 337.
5. H. Tanei and Y. Kondo: *ISIJ Int.*, **57** (2017), 506.
6. S. Hayashi, K. Mizumoto, S. Yoneda, Y. Kondo, H. Tanei and S. Ukai, Oxid. Met., 81 (2014), 357.
7. Y. Shizukawa, S. Hayashi, S. Yoneda, Y. Kondo, H. Tanei and S. Ukai, Oxid. Met., 86 (2016), 315.
8. S. Yoneda, S. Hayashi, Y. Kondo, H. Tanei and S. Ukai, Oxid. Met., 87 (2017), 125.
9. S. Hayashi, S. Yoneda, Y. Kondo, and H. Tanei, Oxid. Met., 94, (2020), 81.
10. B. Gleeson, S. M. M. Hadavi and D. J. Young, Mater. High Temp., 17 (2000), 311.
11. R.Y. Chen and W.Y.D. Yuen, Oxid. Met., 53, (2000), 539.
12. R.Y. Chen and W.Y.D. Yuen, Oxid. Met., 56, (2001), 89.
13. S-N. Lin, G-C. Hung, M-T. Wu, W-L. Wang, and K-C. Hsieh, Steel Res. Int., 88, (2017), #https://doi.org/10.1002/srin.201700045
14. G-M. Cao, T-Z. Wu, R. Xu, Z-f. Li, F-X. Wang, and Z-Yu. Liu, J. Iron Steel Res. Int., 22, (2015), 892.
15. S. Corkovic and A.R. Pyzalla, Mater. Corr., 55, (2004), 341.
16. S. Taniguchi, T. Shibata, M, Murakoshi, Boshoku Gijutsu, 36, (1987), 299 (Japanese).
17. H. Tanei and Y. Kondo, ISIJ int., 57, (2017), 506.
18. T.E. Mitchell, D.A. Voss, and E.P. Butler, J. Mater. Sci., 17, (1982), 1825.
19. C. Juricic, H. Pinto, D. Cardinali, M. Klaus, Ch. Genzel, A.R. Pyzalla, Oxid. Met., 73, (2010), 115.
20. K. Sasaki, K. Hayashi, M. Takeda, S. Nakakubo, Y. Yamada, A. Kitahara, R. Wada, and I. Saeki, Mater. Trans., 61, (2020) 136.
21. S. Hayashi, Y. Takada, I. Saeki, A. Yamauchi, Y. Nishiyama, T. Doi, S. Kyo, and M. Sato, Mater. Corr., 63, (2012) 862.
22. S. Hayashi, Y. Takada, S. Yoneda, and S. Ukai, Oxid. Met., 86, (2016) 151.
23. N. Bertrand, S. Desgranges, D. Poquillon, M.C. Lafont, D. Monceau, Oxid. Met., 73, (2010), 139.
24. S. Taniguchi, Trans. ISIJ, 25, (1985), 3.
25. Y. Tomota, P. Lukáš, D. Neov, S. Narjo, Y.R. Abe, Acta Mater., 51, (2003) 805.
26. M.R. James, in Advances in Surface Treatments, vol.4, Pergamon press., (1987) pp. 349.
27. S. Takaki, T. Masumura, and T. Tsuchiyama, Testu-to-Hagane, 105, (2019), 935 (Japanese).
28. A. Kagawa, T. Okamoto and H. Matsumoto, Acta Metall. 35, (1987), 797.
29. T. Takeuchi, R. Honda, K. Iwayama, and T. Taoka, J. J. App. Phy., 6, (1967), 1282.
30. K. Nishino and H. Honma, Tetsu-to-Hagane, 57, (1971), 954.

[Caption list]

Figure 1 Temperature profiles for the isothermal oxidation at 700 °C in air followed by isothermal transformation at (a) 380 °C and (b) 500 °C then 380 °C.

Figure 2 In situ high-temperature X-ray diffraction patterns of the oxide scale formed during isothermal oxidation at 700 °C for 15 min followed by isothermal transformation at 380 °C in air.

Figure 3 Variation of the intensities of the diffraction signals from the oxide phases during isothermal oxidation at 700 °C followed by isothermal transformation at 380 °C (a) without and (b) with intermediate heat treatment at 500 °C.

Figure 4 (a)–(d) Cross-sectional SEM images of the oxide scale formed at the time points indicated by the letters (i)–(iv) in Fig. 3a. (e) Enlarged SEM image of the region indicated by the white rectangle in panel (c).

Figure 5 (a) Cross-sectional SEM image of the oxide scale formed after isothermal transformation at 380 °C with intermediate heat treatment at 500 °C. (b) Enlarged SEM image of the region indicated by the white rectangle in panel (a).

Figure 6 Variation of the *d*-spacings of the oxide phases during isothermal oxidation at 700 °C and isothermal transformation at 380 °C (a) without and (b) with intermediate heat treatment at 500 °C.

Figure 7 Diffraction peaks of the Fe_3O_4(008) reflection at various ψ angles after isothermal transformation at 380 °C for approximately (a) 20 min and (b) 40 min.

Figure 8 Variation of the *d*-spacing of the Fe_3O_4(008) reflection as a function of $\sin^2\psi$ during the initial stage of isothermal transformation at 380 °C in air: (a) 7 min, (b) 10 min, (c) 13 min, (d) 16 min, (e) 20 min, and (f) 40 min. The closed red circle in each plot indicates the last measurement of each set of $\sin^2\psi$ measurements at $\psi = 0$.

Figure 9 Variation of the gradient *M* for the Fe_3O_4 and Fe reflections as a function of time during isothermal oxidation at 700 °C followed by isothermal transformation at 380 °C.

Figure 10 (a) Variation of the gradient *M* for the Fe_3O_4 and Fe reflections as a function of time during isothermal oxidation at 700 °C followed by isothermal transformation at 380 °C with intermediate heat treatment at 500 °C. (b) Enlargement of the plot shown in panel (a).

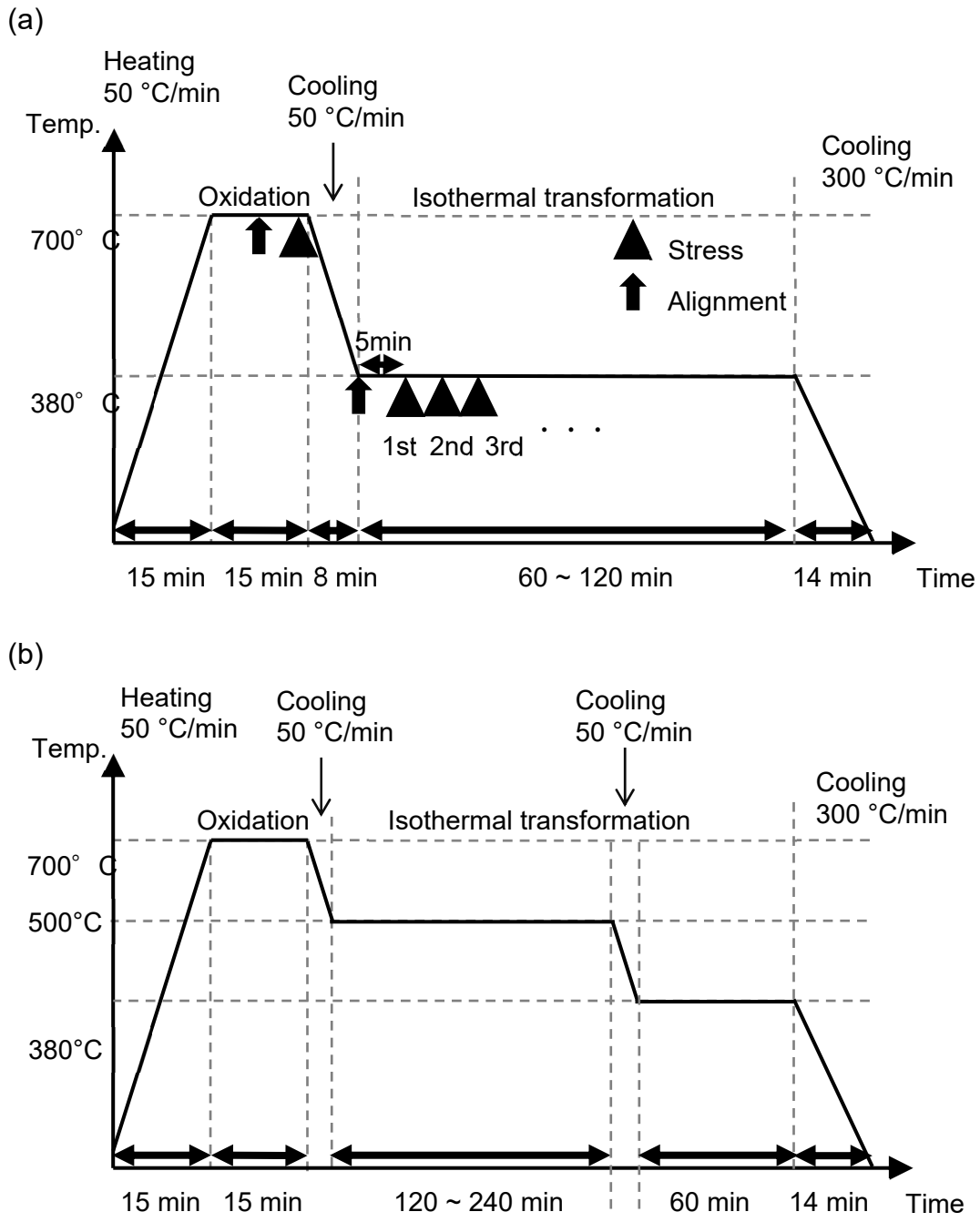

Figure 1 Temperature profiles for the isothermal oxidation at 700 ºC in air followed by an isothermal transformation at different temperatures, (a) 380 ºC and (b) 500 ºC then 380 ºC.

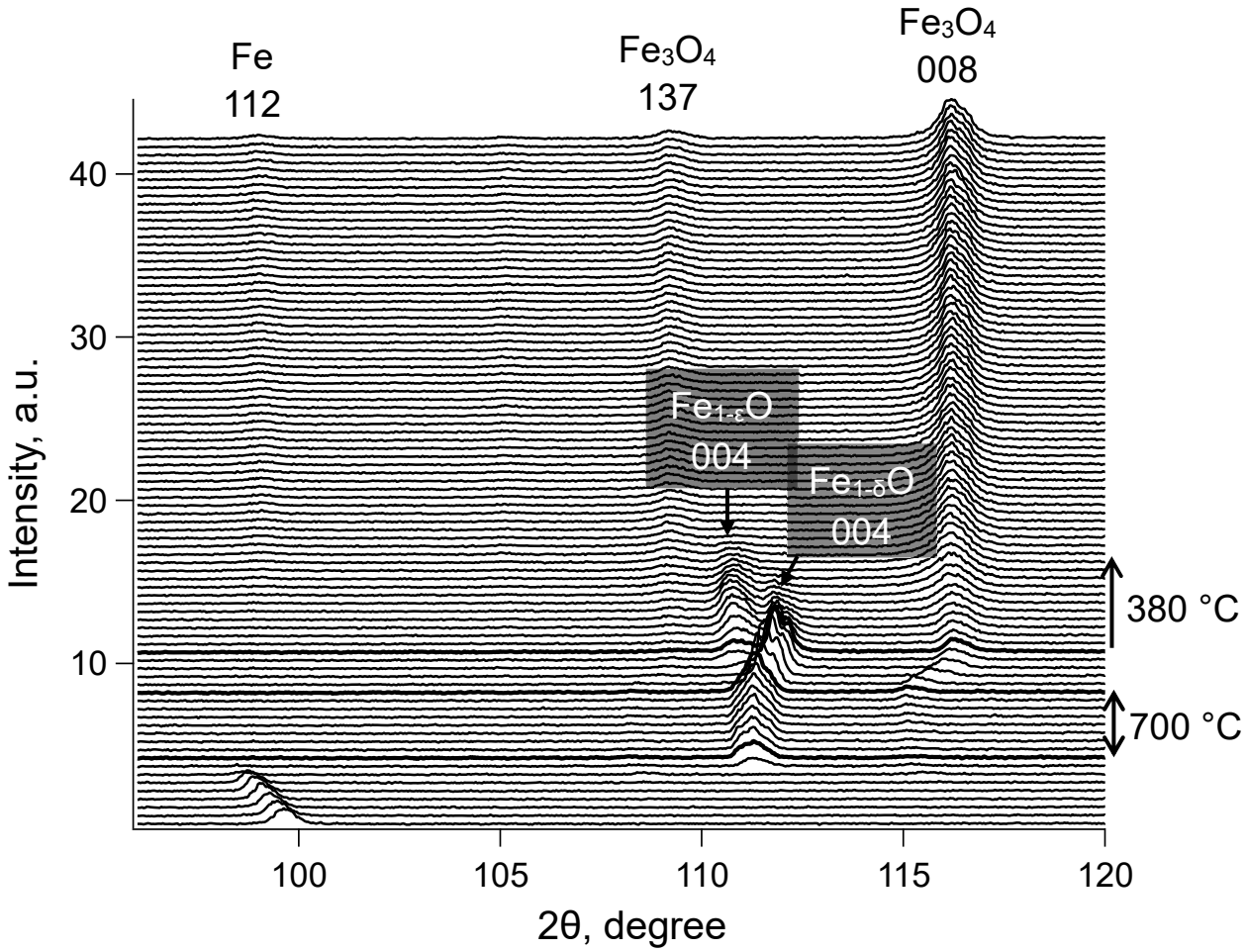

Figure 2 In situ high-temperature X-ray diffraction patterns of the oxide scale formed during isothermal oxidation at 700 °C for 15 min followed by isothermal transformation at 380 °C in air.

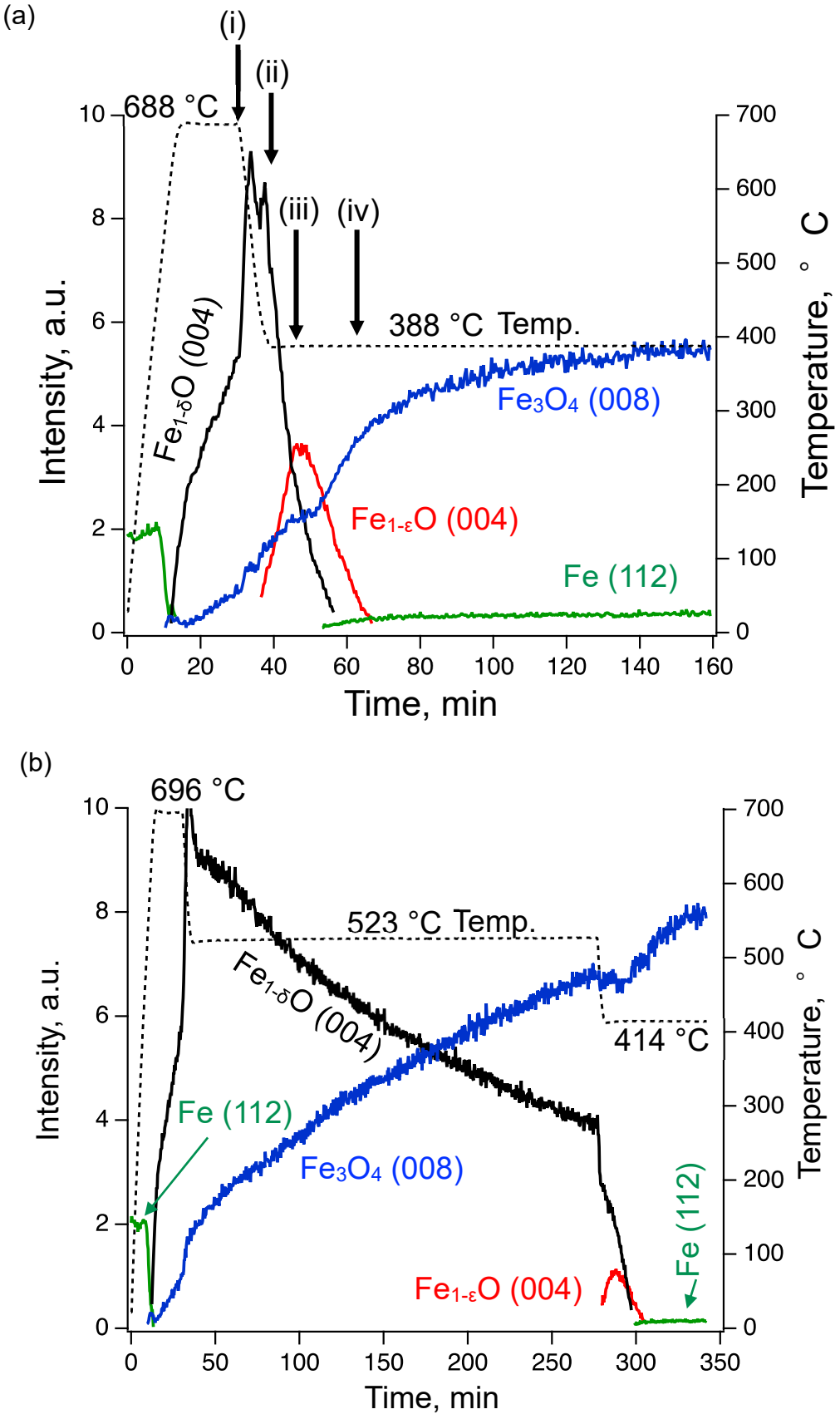

Figure 3 Variation of the intensities of the diffraction signals from the oxide phases during

isothermal oxidation at 700 °C followed by isothermal transformation at 380 °C (a) without and (b) with intermediate heat treatment at 500 °C.

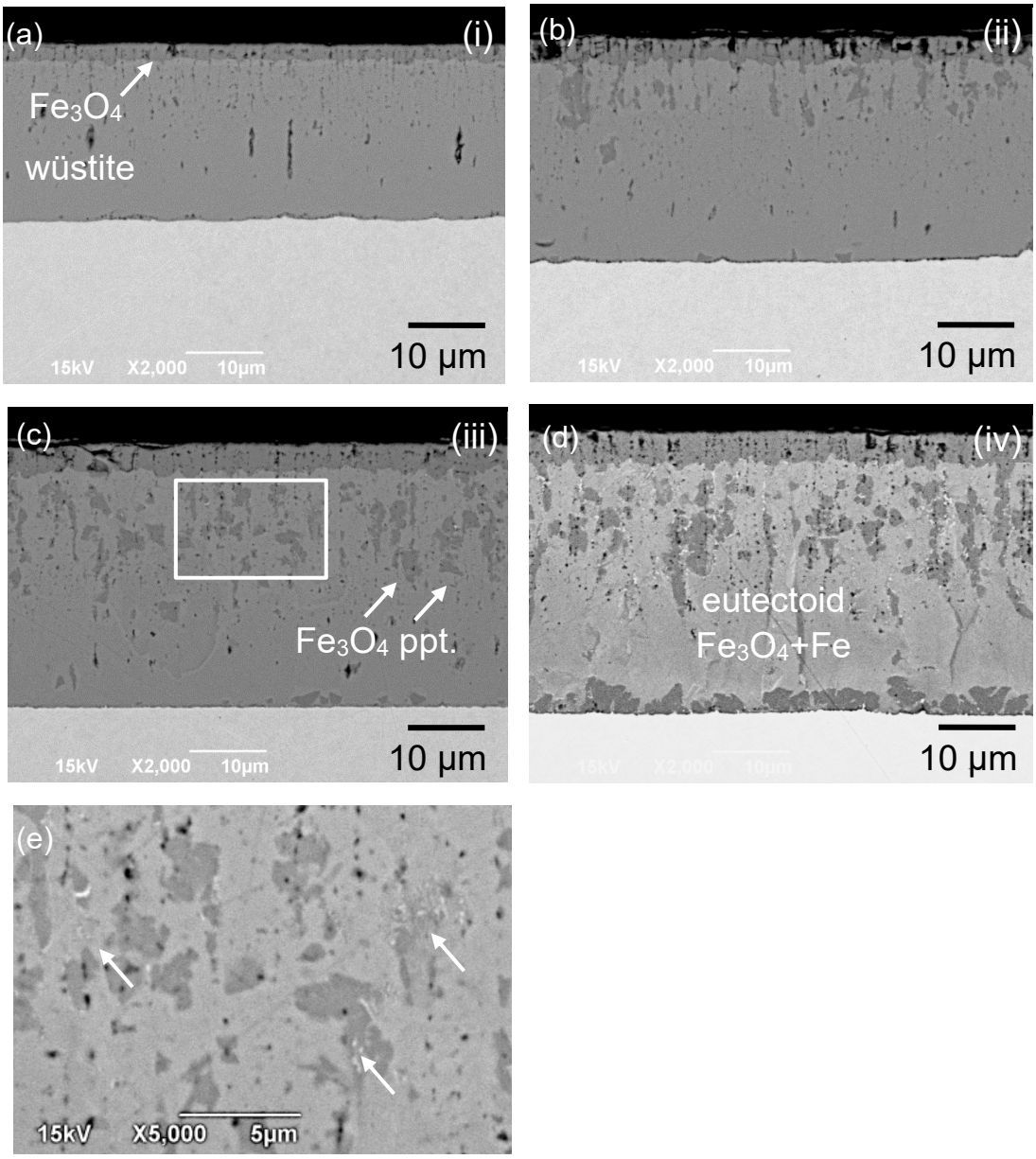

Figure 4 (a)–(d) Cross-sectional SEM images of the oxide scale formed at the time points indicated by the letters (i)–(iv) in Fig. 3a. (e) Enlarged SEM image of the region indicated by the

white rectangle in panel (c).

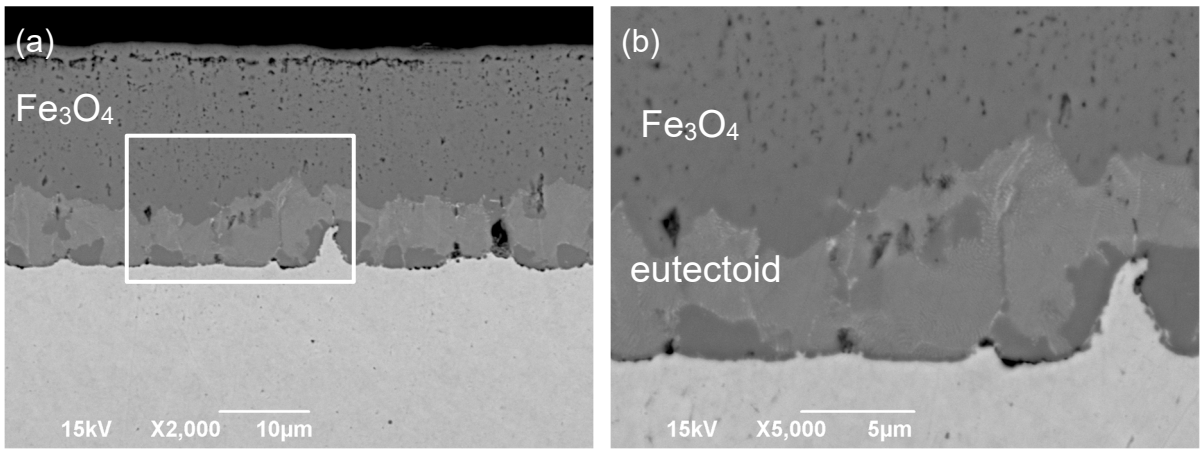

Figure 5 (a) Cross-sectional SEM image of the oxide scale formed after isothermal transformation at 380 °C with intermediate heat treatment at 500 °C. (b) Enlarged SEM image of the region indicated by the white rectangle in panel (a).

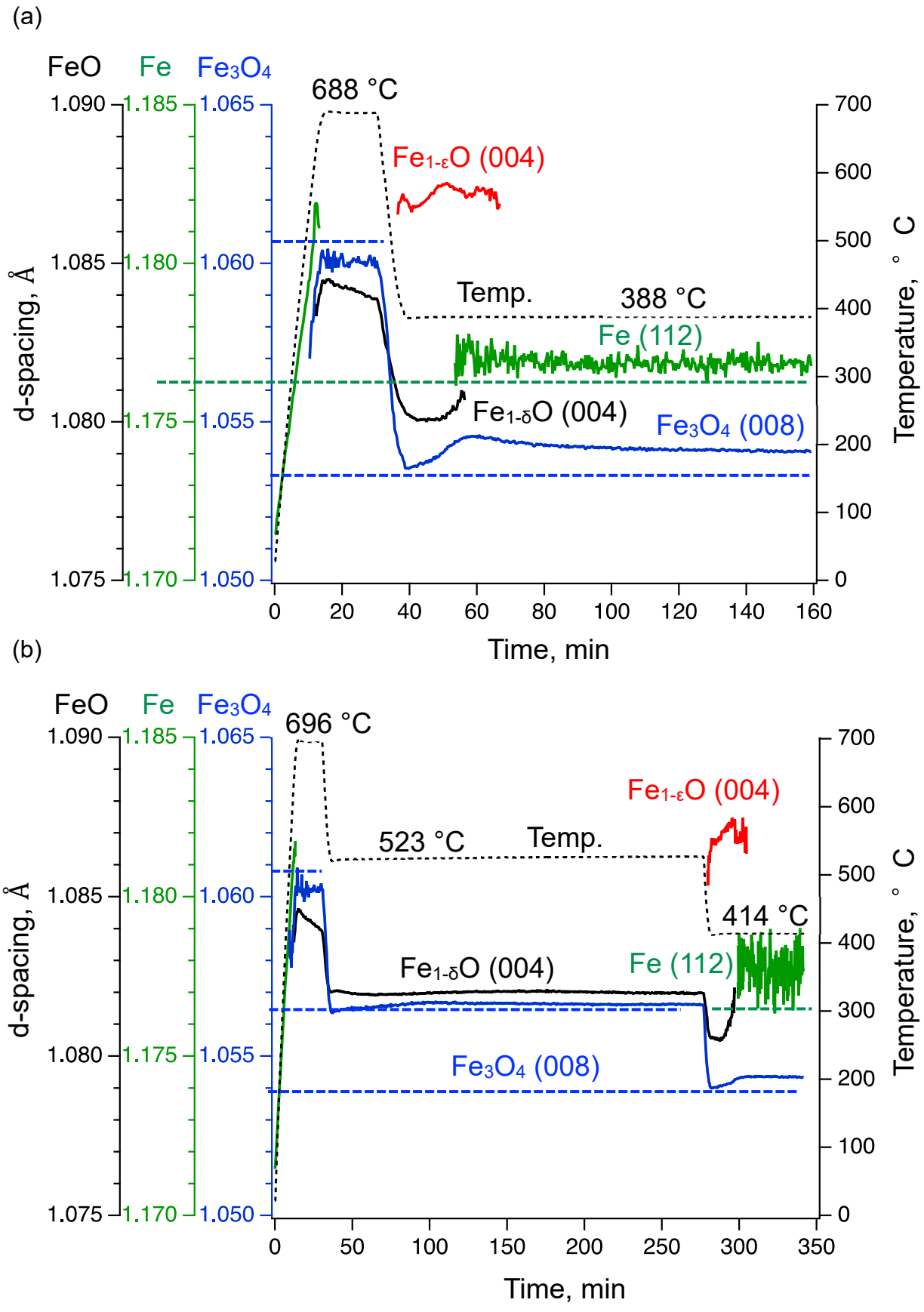

Figure 6 Variation of the *d*-spacings of the oxide phases during isothermal oxidation at 700 °C

and isothermal transformation at 380 °C (a) without and (b) with intermediate heat treatment at 500 °C.

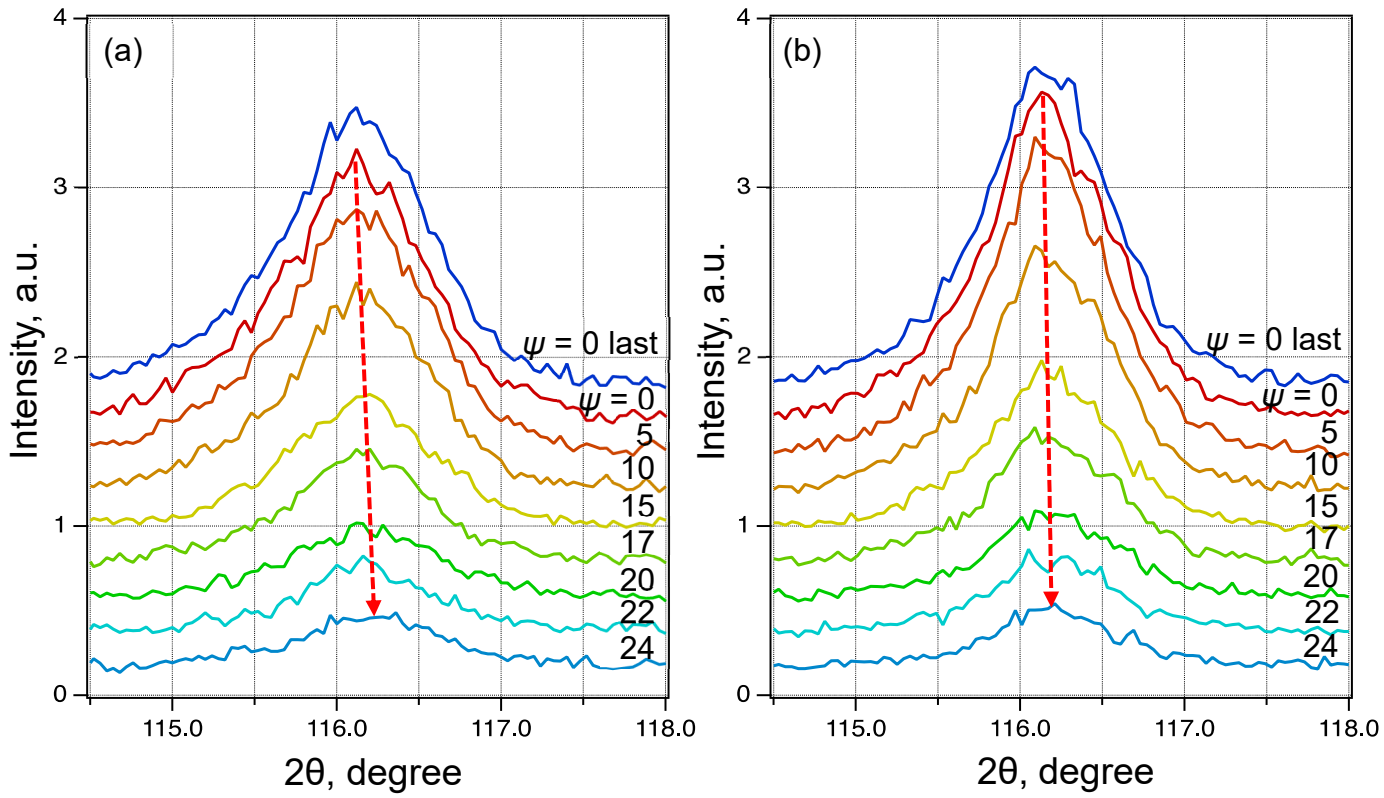

Figure 7 Diffraction peaks of the Fe_3O_4(008) reflection at various ψ angles after isothermal transformation at 380 °C for approximately (a) 20 min and (b) 40 min.

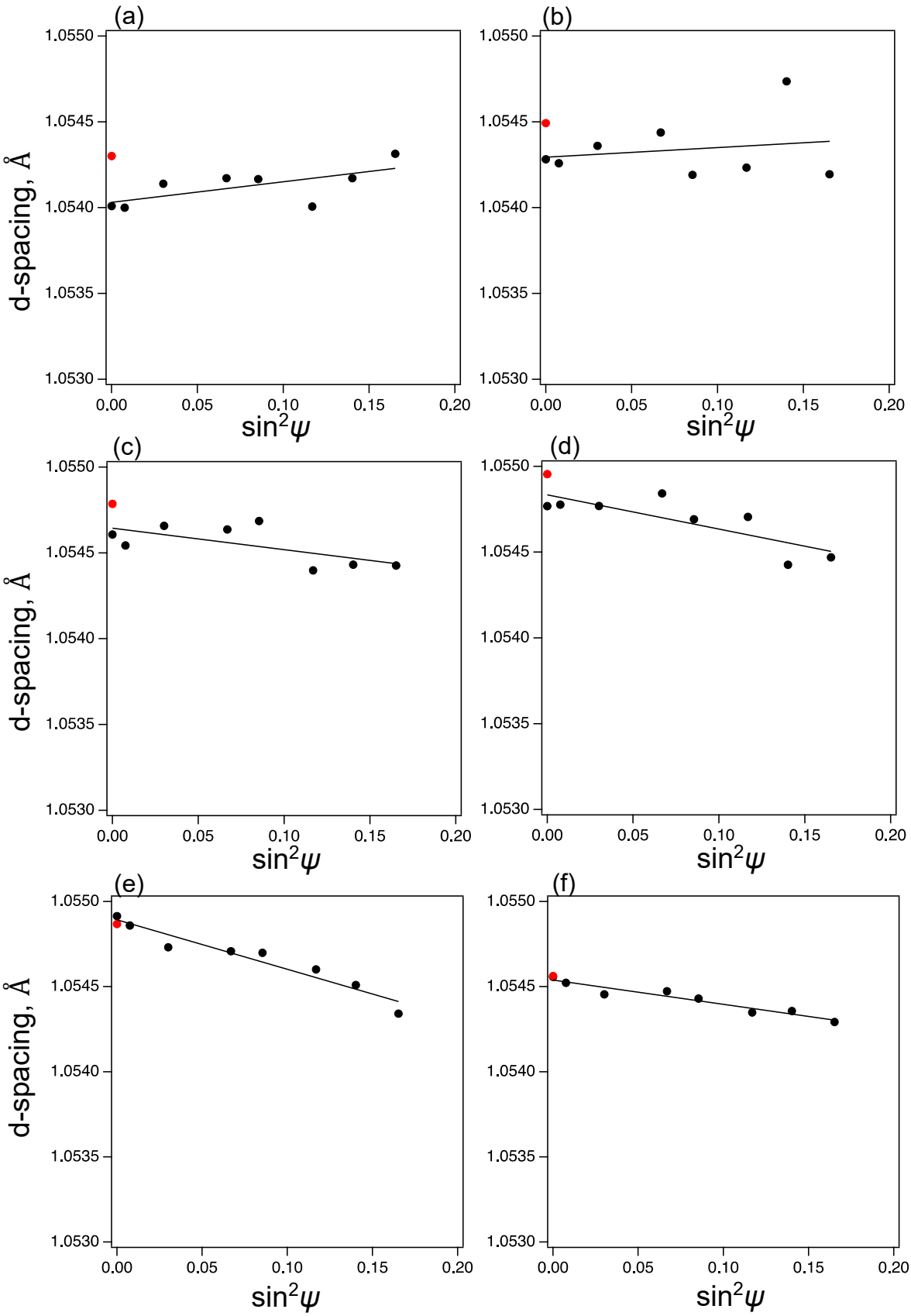

Figure 8 Variation of the *d*-spacing of the Fe_3O_4(008) reflection as a function of $\sin^2\psi$ during the

initial stage of isothermal transformation at 380 °C in air: (a) 7 min, (b) 10 min, (c) 13 min, (d) 16 min, (e) 20 min, and (f) 40 min. The closed red circle in each plot indicates the last measurement of each set of $\sin^2\psi$ measurements at $\psi = 0$.

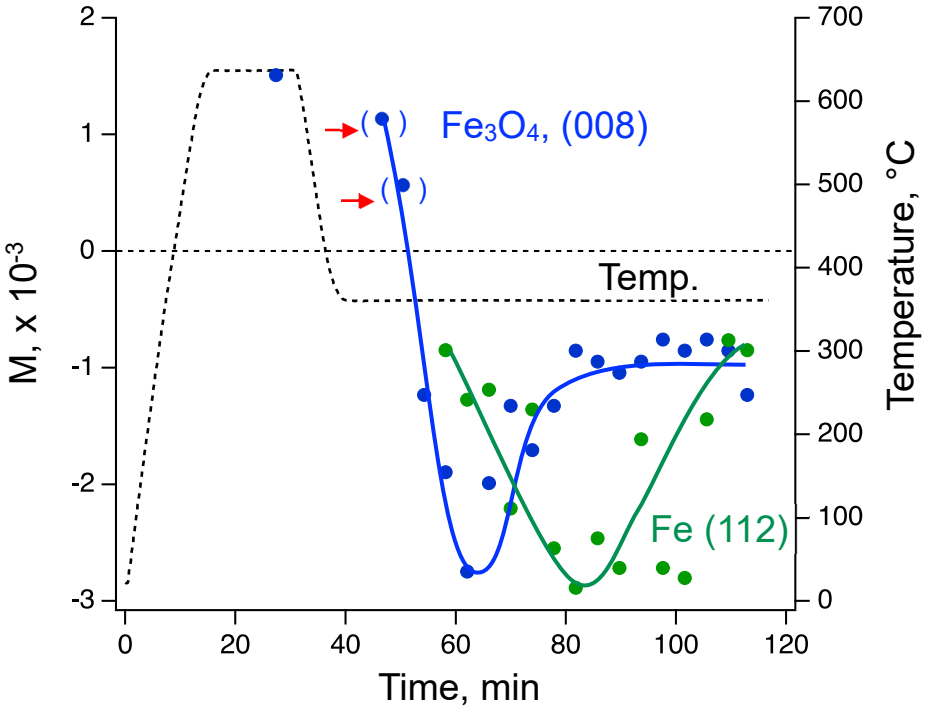

Figure 9 Variation of the gradient M for the Fe_3O_4 and Fe reflections as a function of time during isothermal oxidation at 700 °C followed by isothermal transformation at 380 °C.

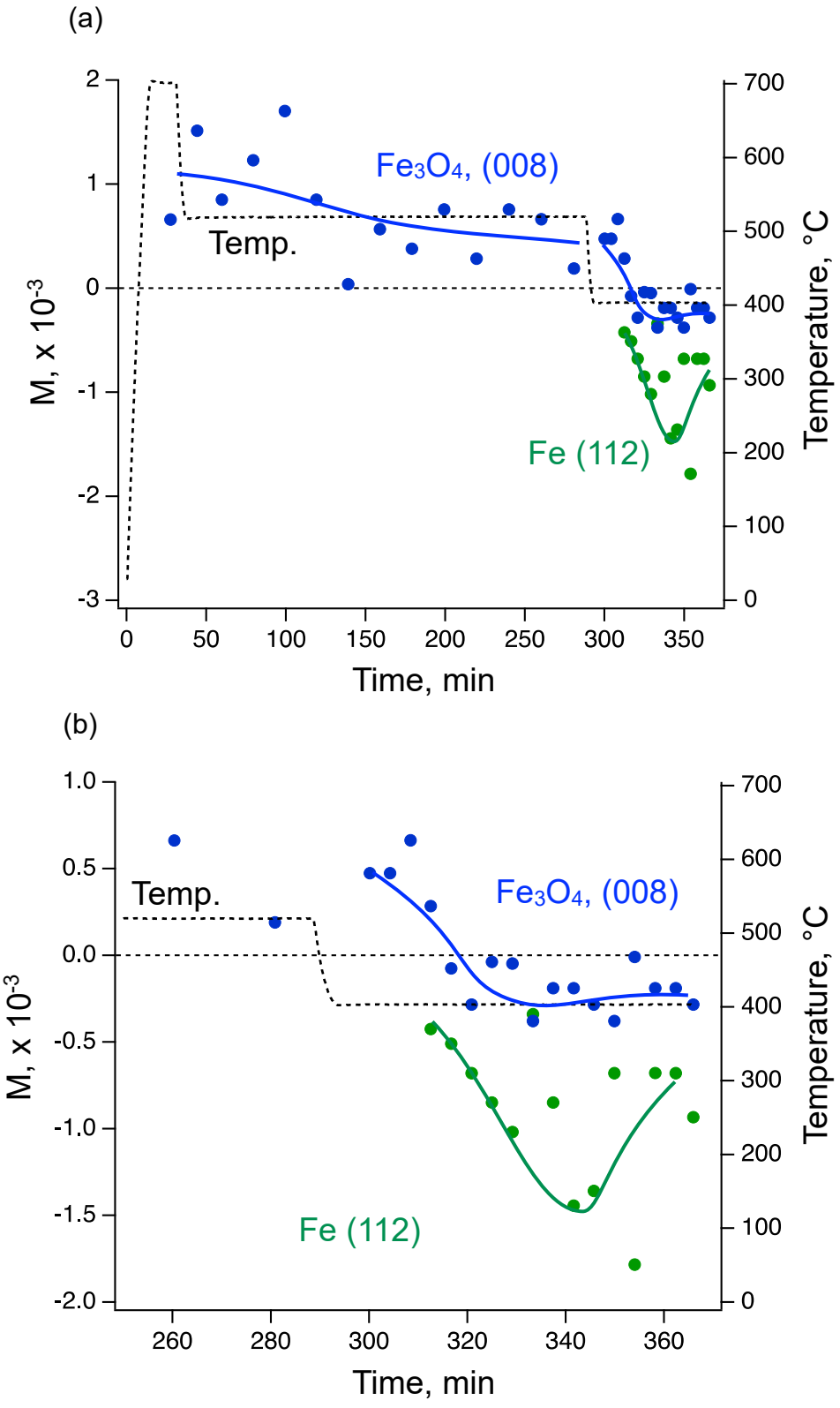

Figure 10 (a) Variation of the gradient *M* for the Fe_3O_4 and Fe reflections as a function of time

during isothermal oxidation at 700 °C followed by isothermal transformation at 380 °C with intermediate heat treatment at 500 °C. (b) Enlargement of the plot shown in panel (a).